Tensile Experiments and Digital Image Correlation of 6061 Aluminum, 304 Steel, and 1018 Steel, and Vibration Experiments of a Cantilever Aluminum Beam

Trevor Burgoyne, AEM 4602W, Lab Group 3Bi

9 December 2022

Abstract

This report details the results of tensile tests performed on dog-bone samples made of three materials: 6061 Aluminum, 304 Steel, and 1018 Steel. Several properties of these materials are computed from the strain-stress curve and are compared to published data, with some variation from the expected results. The properties derived from the Aluminum experiment demonstrated good agreement, while the two steel tests strayed considerably from published values. Sources of experimental error are discussed, such as the slipping of the samples during several of the tests. Recommendations are made as to how best to reduce error during similar tensile tests. Digital Image Correlation (DIC) results from the 1018 Steel tensile test are presented, and the Poisson Ratio is calculated and compared to published values, with some general agreement. Some snapshots of the strain contour plots are examined and compared to what is expected from theory, with very good agreement. Vibration experiments performed using a cantilever Aluminum beam are detailed, with natural frequencies being derived from the experimental data and compared to theory, with overall agreement for the first five modes.

Introduction

Tensile tests are often used to derive and verify key properties of a select material to gauge its applicability for a specific application. Much room exists for repeating these tests and expanding on the areas of investigation, such as is seen in [1] which examines various properties of 6061 Aluminum and how they vary with different factors, such as sample thickness. Large datasheets and other collections that detail the properties of various materials, as seen in [2], are constantly in demand and are meticulously updated so as to provide interested parties with a general understanding of how materials compare. Even still, the more general that these values become, the less accurately they predict the behavior of samples that differ from the average. As such, tensile testing of actual samples remains a staple of material testing and selection. With the advancements made in computer vision technology in recent years, new ways of calculating quantities such as Poisson's ratio have emerged. Digital Image Correlation (DIC) is one such technology that has been used to characterize material properties that were otherwise very difficult to measure, as is discussed in [3]. And in light of high-profile structural failures that have been caused by the unforeseen effects of resonance, an analysis of the natural frequencies of structures is a staple of modern engineering projects. The vibration tests conducted in this experiment seek to validate the theory used to derive these natural frequencies.

The tensile tests detailed in this report are used to determine a wide range of material properties from the stress-strain curve collected by the experiment. Engineering stress (σ) is defined as the

ratio of force to the cross-sectional area, while the engineering strain (ε) is the ratio of the elongation of a sample to its original, undeformed length. When plotting stress vs strain, the initial linear portion of the response is referred to as elastic deformation, since the deformation is completely reversible. The slope (σ/ε) of this elastic region is defined as Young's Modulus, or Elastic Modulus (E). The stress that marks the end of this elastic behavior is the yield stress (σ_y), which is conventionally defined as the stress which causes a plastic strain of 0.2%. Once the applied load exceeds this yield stress, the sample begins to plastically deform, and stress continues to increase in a non-linear fashion until it reaches the ultimate stress, also known as the ultimate strength (σ_u). After passing this ultimate stress, the stress begins to decrease as the material begins necking, meaning that the cross-sectional area begins to decrease at a point along the sample until it ultimately fractures. The ratio of the cross-sectional area at the point of fracture to the undeformed cross-sectional area is known as the percent reduction in area at failure (% RA). The true strain at failure (ε_f) is defined as the natural log of the ratio of the instantaneous length to the undeformed length of the sample, assuming zero volume change. Toughness is the ability of a material to absorb energy in the process before fracture, and is calculated as the area under the stress-strain curve up until failure.

The Digital Image Correlation (DIC) test performed takes advantage of advances in computer vision algorithms to track the relative motion of a speckled dog-bone sample under a tensile load. The movement of small areas from frame to frame is deduced by searching nearby pixels in future frames and computing a similarity score by using a sum of squared differences. By tracking the motion of the individual speckles from frame to frame, a heat map of the horizontal and vertical strains (ε_{xx} and ε_{yy}) is generated. Poisson's Ratio (ν) is defined as negative the ratio of the rate of change of ε_{xx} over the rate of change of ε_{yy}, or in other words relates how displacement in one dimension is linked to displacement in the other.

The vibration analysis in this report focuses on the identification of natural frequencies (ω_n) and mode shapes of a cantilever aluminum beam. From the Euler-Bernoulli Beam equation, an expression of the natural frequency can be derived as:

$$\omega_n = z^2 * \sqrt{\frac{EI}{mL^4}}$$

where E is the Elastic Modulus of the beam material, I is the moment of Inertia of the beam cross-section, m is the mass, L is the beam length. The equation cosh (z) cos(z) + 1 = 0 defines the possible values of z, where the first three roots are approximately z_n = 1.875, 4.694, 7.855 (n = 1,2,3), where n refers to the mode number. The mode number is related to the number of nodes (or stationary points) that occur during vibrations at that natural frequency, with the number of nodes being equal to one less than the mode number.

This lab had various purposes spread across the two main types of experiments. For the tensile experiments, the objective was to experimentally determine the material properties of different metal samples, such as the Young's Modulus, Poisson's Ratio, etc. and to compare these derived properties to published data where possible. Additionally, the in-plain strain components were to be calculated from the full-field digital image correlation measurements made using the DIC camera. For the vibration experiments, the frequency response of the cantilever beam was

to be compared to theory, and the natural frequencies of each resonance was to be derived, along with their corresponding mode shapes.

Apparatus & Methodology

The experiment was conducted in two parts, which will be referenced throughout the report as the tensile experiment and the vibration experiment. For the tensile experiment, three metal samples were tested: 6061 Aluminum, 304 Steel and 1018 Steel. The experimental area included a tensile test machine with top and bottom clamps designed to hold dog-bone test samples, and next to it was a computer that received the test data . A separate laptop computer was connected to a Digital Image Correlation (DIC) camera as well as a separate light fixture on a tripod. See the Appendix for images of the test area. An extensometer was first calibrated by attaching it to a micrometer and making repeated measurements of the voltage measured when the micrometer was extended by 0.1 mm. Care was taken to avoid hysteresis by moving the micrometer slightly past the desired position before settling on the value and taking the measurement. Each metal dog-bone sample then had the width, thickness, and length of the test section measured three times at different locations using a digital caliper. One at a time, the metal samples were placed in the top and bottom clamps of the tensile test machine, with care taken to ensure the sample was as secure and straight as possible. Once in position, the tensile machine was zeroed out and a small amount of tension was applied (~20-30 lbs) before beginning the test. The extensometer was attached to the sample, the computer was set to start collecting data, and the tensile machine was started to begin the tensile experiment. The displayed force on the tensile machine was carefully monitored, and once the force began to steadily decrease (indicative of necking) the extensometer was removed from the sample to avoid any damage that might occur when the sample would break. Once the sample yielded, the tensile machine automatically stopped the test and reported the max and final values of force and displacement. The width and thickness of the break in the sample was recorded, and then the process was repeated for all three samples, except for a slight difference in the test with the 1018 Steel. For the 1018 Steel, the DIC camera was used instead of an extensometer, running with a frame rate of 2 frames/second and a resolution of 3.45 μm/pixel. The 1018 Steel sample had a spray-painted speckled pattern to enable later computer vision analysis of the experiment. The DIC camera was positioned such that it captured the whole of the sample with the bottom of the sample being flush with the bottom of the frame. The light was positioned close enough to the sample to make it fully visible. The laptop connected to the camera ran IDS software that was used to view the DIC camera feed, and the focus was adjusted on the camera to make sure the speckles were as well defined as possible. Once the recording was started on the laptop and the other computer also began collection, the tensile test was run just as before, and was run until the sample broke and the test automatically ended.

The vibration experiment area contained a shaker (historically used for experiments involving aerodynamic flutter) with an accelerometer connected at the free end of a cantilever beam, whose dimensions are detailed in the Appendix calculations. The accelerometer was connected to an oscilloscope through a signal amplifier, and then connected to a separate function generator that was connected via the local network to a desktop computer. See the Appendix for images of the test area. Four different tests were performed, and each only required the test to

be selected on the computer and then sent to the function generator. Once sent, a button was pressed on the generator to pull the command from the local network, and the test was run. The first two tests were white and pink noise tests respectively, where a large range of frequencies were all generated simultaneously, and the magnitude of the accelerometer response was graphed after performing a Fast Fourier Transform (FFT) on the raw data. The next two tests were sinusoidal frequency sweeps of 0-10 Hz and 0-200 Hz respectively. The results of all four tests gave clear indications of candidates for the natural frequencies and mode shapes of the cantilever aluminum beam that was attached to the shaker.

For the tensile test, all the dog-bone samples were anticipated to be the exact same dimensions since they were all cut using the same outline. Some redundant measurements were taken and the averages, and this assumption held true (for example, the cross-sectional area of the 6061 Aluminum and the 304 Steel came out to be exactly the same even though they were measured separately). For the true strain at failure, zero volume change is assumed to simplify the calculations, which is generally true but not exactly correct, but is a close enough approximation since any volume change would be small compared to the magnitude of the strain. Additionally, the toughness of each material was calculated using numerical integration and the trapezoidal rule, since the experimental data does not follow any trivial analytical equation. For the DIC measurements, the sample surface was assumed to be planar, with no movement toward/away from the camera. This assumption is valid since the camera was set up such that visually it appeared to capture only the forward-facing plane of the sample, and any slight offset is insignificant in comparison to the actual motion of the speckles in the sample as the experiment ran. Also, only 2D motion could be captured anyways since only one camera was used, so this assumption was unavoidable. For the vibration experiments, the shaker and aluminum bar were modeled as a cantilever beam with no motion at the end attached to the shaker apparatus. This assumption is valid since the shaker was very heavy and unlikely to move at all during the experiment, even at resonance, and this was observed to be true during the tests.

Uncertainties for the vibration experiments are not considered in this report for the sake of brevity, since the frequency response plots are very noisy. Thus all values are reported to two significant figures. For the tensile experiments, Table 1 below describes the uncertainties used for all the directly measured quantities. The propagation of error is discussed in the Appendix and presented together with calculated values in the Results section.

Description	Load	Creep Load	Crosshead Position	Extensometer	Caliper
Uncertainty	± 5 lbs + 4%	± 0.5 lbs	± 0.5 in	± 4%	± 0.005 in

Table 1: Uncertainty for various measured values.

For the tensile tests, the calculated material properties for each of the three metals used was expected to be similar to those found in material data sheets or published figures. Aluminum was anticipated to demonstrate a much lower yield strength, ultimate strength, and toughness

than the two Steels, since Aluminum is a weaker material. Additionally, the Steels were expected to have a region of relatively constant stress after yielding and before beginning to neck. The expected data is presented and compared to the experiment in the Overall Discussion of the Results section. For the vibration tests, the theoretical natural frequencies for the first five mode shapes were calculated using the formulas described in the Introduction, with the specific material properties (Elastic Modulus, density) of the Aluminum being taken from public data sheets. The natural frequencies from theory were calculated as 4.5, 28, 78, 150, and 250 Hz. Details of that calculation are in the Appendix.

Results

Material Properties

Using the data collected from the tensile tests, several material properties were calculated as described in the Introduction. The details of these calculations are included in the Appendix, and the results are presented in Table 2 below.

Material	E (GPa)	ν (elastic)	ν (plastic)	σ_y (MPa)	σ_u (MPa)	% RA	ε_f	Toughness (MPa)
6061 Aluminum	76.4 ± 6.11	N/A	N/A	265.6 ± 21.2	344.9 ± 27.6	40.6 ± 3.25	0.52 ± .04	23.00
304 Steel	198.3 ± 15.9	N/A	N/A	367.5 ± 29.4	463.5 ± 37.1	54.3 ± 4.34	0.78 ± .06	81.74
1018 Steel	237.4 ± 19.0	.10 ± .03	.42 ± .04	400.8 ± 32.1	540.8 ± 43.3	54.7 ± 4.38	0.79 ± .06	934.8

Table 2: Material Properties calculated from tensile test data. Calculation details in the Appendix.

The Poisson's ratios (ν) presented in Table 2 for the 1018 Steel sample were calculated using the results of the DIC analysis. To convey the general trends in the strains evaluated in this analysis, snapshots of the strain contour plots will be presented before and after yielding, as well as just before fracture. Before yielding (Figures 1-2, see Appendix), both strain components (ε_{xx} and ε_{yy}) appear fairly uniform throughout the samples. Just after yielding (Figures 3-4), regions of varied strains begin to appear, and the region of highest strain appears to be close to the center of the sample. Finally, in the moments just before failure (Figures 5-6), the center of the sample is experiencing a very high level of strain in the exact region where the fracture ultimately occurred. The relative level of strain decreases steadily and uniformly as you get further away from the point of fracture along the sample, in contrast to the less uniform distribution previously seen in Figures 3-4. See the Appendix for the Figures in question.

Vibration

As discussed in the Apparatus & Methodology section, the vibration experiments utilized a shaker that had an accelerometer connected at the free end of a cantilever beam. The shaker was controlled by a function generator that was connected via the local network to a desktop computer. Four different tests were performed based on commands sent to the function

generator from the computer. The first two tests were white and pink noise tests respectively, where a large range of frequencies were all generated simultaneously, and the magnitude of the accelerometer response was graphed after performing a Fast Fourier Transform (FFT) on the raw data. The next two tests were sinusoidal frequency sweeps of 0-10 Hz and 0-200 Hz respectively, which allowed the first few resonances to be verified.

Using the results from these four experiments, the first five natural frequencies were identified as shown in Table 3. The first mode was clearest in the 0-10 Hz scan, the second through fourth were present in the 0-200 Hz sweep, and white/pink noise tests clearly captured the second through fifth modes.

Mode #	**1**	**2**	**3**	**4**	**5**
Natural Frequency (Hz)	4.0	25	71	140	230

Table 3: Natural Frequencies for the first five mode shapes, calculated from the vibration test data. Calculation details in the Appendix.

After estimating the natural frequencies of the beam using this method, the shaker was set to run specifically at these frequencies in a dark room while a strobe light was set to shine on the vibrating beam at the exact same frequency, which allowed for a very clear view of the different mode shapes and the resulting node locations along the beam. At each mode, the number of stationary nodes on the beam was equal to one minus the mode number (i.e. mode two had one node, mode three had two nodes, etc.).

Overall discussion

Using the equation for ω_n discussed in the Introduction, the theoretical natural frequencies for the first five modes were calculated and are compared to the experimental results in Table 4:

Mode #	**1**	**2**	**3**	**4**	**5**
From Data (Hz)	4.0	25	71	140	230
From Theory (Hz)	4.5	28	78	150	250

Table 4: Theoretical and Experimental estimates of the natural frequencies for the Aluminum cantilever beam. Calculates are detailed further in the Appendix.

Overall there is substantial agreement between the actual and theoretical values in Table 5, with a consistent over-estimation present in the theoretical calculations. One oversight made in the data collection was that the mass of the accelerometer was not recorded, so the slightly larger mass in the actual experiment could explain part of this discrepancy. Additionally, the exact composition of the Aluminum present was not investigated in detail, and standard published values for material properties were used, which probably played a significant role in the overestimation. Yet the relatively close agreement between the two data sets indicates that the

underlying theory faithfully models the fundamental mechanics at play in the vibration experiment.

For the tensile tests, the most readily available published data on the material properties calculated in Table 2 are Young's Modulus (E), Poisson's ratio (ν), yield stress (σ_y), and ultimate strength (σ_u). Table three compares the experimental values for these select properties to those found in various publications:

Material & Source	**E (GPa)**	**ν (elastic)**	**ν (plastic)**	**σ_y (MPa)**	**σ_u (MPa)**
6061 Aluminum from Table 2	76.4 ± 6.11	N/A	N/A	265.6 ± 21.2	344.9 ± 27.6
6061 Aluminum from [1]	69.8 ± 1.5	N/A	N/A	277.6 ± 8.3	319.8 ± 16.2
304 Steel from Table 2	198.3 ± 15.9	N/A	N/A	367.5 ± 29.4	463.5 ± 37.1
304 Steel from [2]	193	N/A	N/A	215	505
1018 Steel from Table 2	237.4 ± 19.0	.10 ± .03	.42 ± .04	400.8 ± 32.1	540.8 ± 43.3
1018 Steel from [2]	200	.29	.50	370	440

Table 5: Selected values from Table 2 are compared to published data.

The Aluminum properties derived from the experimental data showed good agreement with the values presented in [1], with E, σ_y, and σ_u all falling within one error bar of each other. This was by far the most successful of the tests, with no significant slippage occurring during the procedure. The overall shape of the stress-strain curve (found in the Appendix) also matches very well with the curves presented in [1].

The 304 Steel properties derived from the experimental data showed some good and poor agreement with published values as seen in [2], with both E and σ_u falling within one error bar but σ_y being significantly larger than was expected. The wildly different value for yield stress is likely due to a combination of two issues that occurred during data collection. First, the sample slipped just as it began to yield, and due to this slippage the extensometer must have also slipped somewhat because the raw extensometer data shot down to zero for several ticks. But even considering this slippage, the stress-strain curve shows that the elastic deformation continued well past the published value of 215 MPa. Perhaps the 304 Steel in this experiment differed in some way with the alloy considered [2], or it could also be that the stress values were calibrated incorrectly such that they gave values that were too large. Even with these issues, the general shape of the stress-strain curve (included in the Appendix) seems to agree with theory, and shows a noticeable region of no stress increase right after yielding.

The 1018 Steel properties derived from the experimental data showed somewhat poor agreement with the values presented in [2], with E, σ_y, σ_u,and ν all falling within two or more error bars. The DIC footage confirmed that significant horizontal slippage occurred during the elastic portion of the deformation, which is likely the main contributing factor in the error from the experimental results, especially for the Elastic Modulus and Poisson's Ratio calculations. However, the general shape of the stress-strain curve (included in the Appendix) agrees with theory, and shows a region of no stress increase right after yielding, even if it does seem to actually decrease due to slippage.

When comparing the properties of the Aluminum and Steel alloys, several key differences stand out. In terms of overall strength, which can be characterized by looking at a combination of yield strength, ultimate strength, elastic modulus, and toughness, Steel is clearly a stronger material than Aluminum. This means that it can withstand more stress before yielding or failing, making it superior for applications where high stress is anticipated. Aluminum also has a ~15% lower Reduction in Area (RA) at the point of fracture, meaning that it is less ductile and can experience less plastic deformation before fracturing. Given all of these factors, it would seem that Steel is clearly the superior material, but these characteristics don't take into account other key factors such as density or cost. Aluminum is of course much less dense than Steel, making it a popular material for Aerospace applications where less weight can provide large improvements in fuel efficiency. So even though it may objectively be a weaker material, if it is strong enough to withstand the anticipated stresses, Aluminum is used in many different applications due to its other inherent advantages.

Conclusion

This report details the results of tensile tests performed on dog-bone samples made of three different metals. Several properties of these materials were computed from the strain-stress curve and compared to published data, with significant variation from the expected results. While the expected differences between the Aluminum and Steel samples were confirmed (i.e. higher yield strength, etc. in the Steels), the numerical results did not have very good agreement with published values. Due to the very limited time in the experiment area, only one test of each metal was performed, and some tests had to be repeated several times due to the dog-bone sample slipping in the tensile test machine. So even though the stress-strain curves ultimately agree with what was anticipated for each material, the specific values were at times far off from what was expected. Future tensile tests should ensure that several repeated tests are performed to help drive down this error, and careful watch of the dog-bone sample during the experiment should be kept so as to immediately identify and work to eliminate any imperfections in the test area that might contribute to slippage. Additionally, Digital Image Correlation results from the 1018 Steel tensile test were presented, and the Poisson Ratio was calculated and compared to published values, with some general agreement. As expected, the Poisson Ratio for the elastic region of the test was much lower than that of the plastic region. However, the actual values of both ratios were lower than expected, especially for the elastic region. Once again, significant slippage of the dog-bone sample could be seen when reviewing the DIC imagery, and this slipping was most prevalent during elastic deformation up until yielding, which

led to a very poor correlation between the horizontal and vertical strains. Yet the snapshots of the strain contour plots examined showed very good agreement with theory, with clear necking being observed around the area where fracture ultimately occurred. The vibration experiments performed using a cantilever Aluminum beam were detailed, with the first five natural frequencies being derived from the experimental data and compared to theory, with overall agreement. The experimental results were slightly lower than expected, but followed the expected mathematical relationship outlined in the Introduction, which variation could be due to not considering the added weight of the accelerometer among other factors that were discussed in the Results section.

Future work should apply the suggestions mentioned previously concerning how to perform more accurate and useful tensile tests, and the test methodology should be repeated and improved until better agreement with published data is reached. Especially in applications where the material properties being investigated are of great importance, care should be taken to verify and double-check results before proceeding with the selection of a material, especially when published data on a specific material is not readily available. The fundamental material properties explored in the tensile experiments build off of the work taken to derive such properties in other courses at the University of Minnesota such as Introduction to the Science of Engineering Materials (MATS 2001), Deformable Body Mechanics (AEM 3031) and Aerospace Structures (AEM 4501). In MATS 2001, we used stress-strain curves to calculate elastic modulus, yield stress, etc. In AEM 4501, these material properties were used in larger structural models to predict when structures would fail and what materials were applicable to certain requirements (i.e. weight, strength, etc). As the demand for new and more advanced materials continues to grow, the use of tensile tests among other methods will be essential in deriving these key properties and allowing for design requirements to be met and verified.

Ethical Discussion

(1) When plotting experimental data, care should be taken to only use the level of precision dictated by the equipment or methods used to collect said data. As such, the correct number of significant digits should be used, even if by not doing so one might generate “better” results. The same could be said of rounding data too aggressively to achieve the same outcome: it is dishonest and a deliberate misrepresentation of the facts. Any points that might not fit an otherwise “nice” correlation should not be discarded. In fact, a few outliers are all but expected to appear. Instead of ignoring them and being dishonest, these points should be explicitly highlighted and a well-reasoned argument should be made as to why they do or don’t invalidate the overall trend. If the points *are* removed for whatever reason, even more attention should be given to any reasoning behind their exclusion, so as to prevent the reader from drawing any incorrect conclusions from the idealized fit. Considerations should be made about the potential use of the presented data in future research and development, since an accumulation of small exclusions could potentially build up to paint a misleading picture that causes future investigations to waste time, money, and even put people in danger based on the faulty information that was presented.

(2) If new information casts doubt on previously collected data or publications, it should be taken seriously and investigated thoughtfully before jumping to conclusions. Once the issue has been substantially verified by multiple parties, those associated with the work in question should be consulted and presented the findings of the investigation so that they can raise any objections to the concerns raised. Once open communication has occurred and the faulty data is still confirmed, a public correction should be made. This will help prevent the propagation of the erroneous publication and will encourage others to reanalyze their use of the results of the project. While this discovery is likely very disappointing and disheartening to those involved in the original research, they could have the opportunity to redo the experiment and actually come up with new and revolutionary results that actually could help to shape future theory and help to confirm or upend commonly held beliefs. For theirs and everyone else's sake the incorrect data should be retracted or corrected as soon as reasonably possible.

(3) As discussed at the end of scenario (2), just because experimental results does/doesn't agree with theory is by no means a justification to prevent its publication. Of course, if several authors and conventional wisdom believes something there may indeed be good reason for it, but history is replete with examples of new discoveries upending centuries of unquestioned dogma. So if care is taken to explain any potential deviation of experimental results from the commonly accepted answers, a contradictory work can be very valuable in moving the public discourse forward. And even if, upon further scrutiny, some inconsistency is discovered that explains away the differences in the new results, that alone could be a valuable contribution to the scientific community by better defining the criteria necessary to make certain assumptions or apply different principles.

References

[1] Shinde, Prakash, et al., (2012). "Critical J-integral of thin aluminium sheets employing a modified single edge plate specimen."

[2] Harvey, Philip, (1982). "Engineering Properties of Steels."

[3] Pritchard, Robyn, et al., (2013). "Precise determination of the Poisson ratio in soft materials with 2D digital image correlation."

Appendix

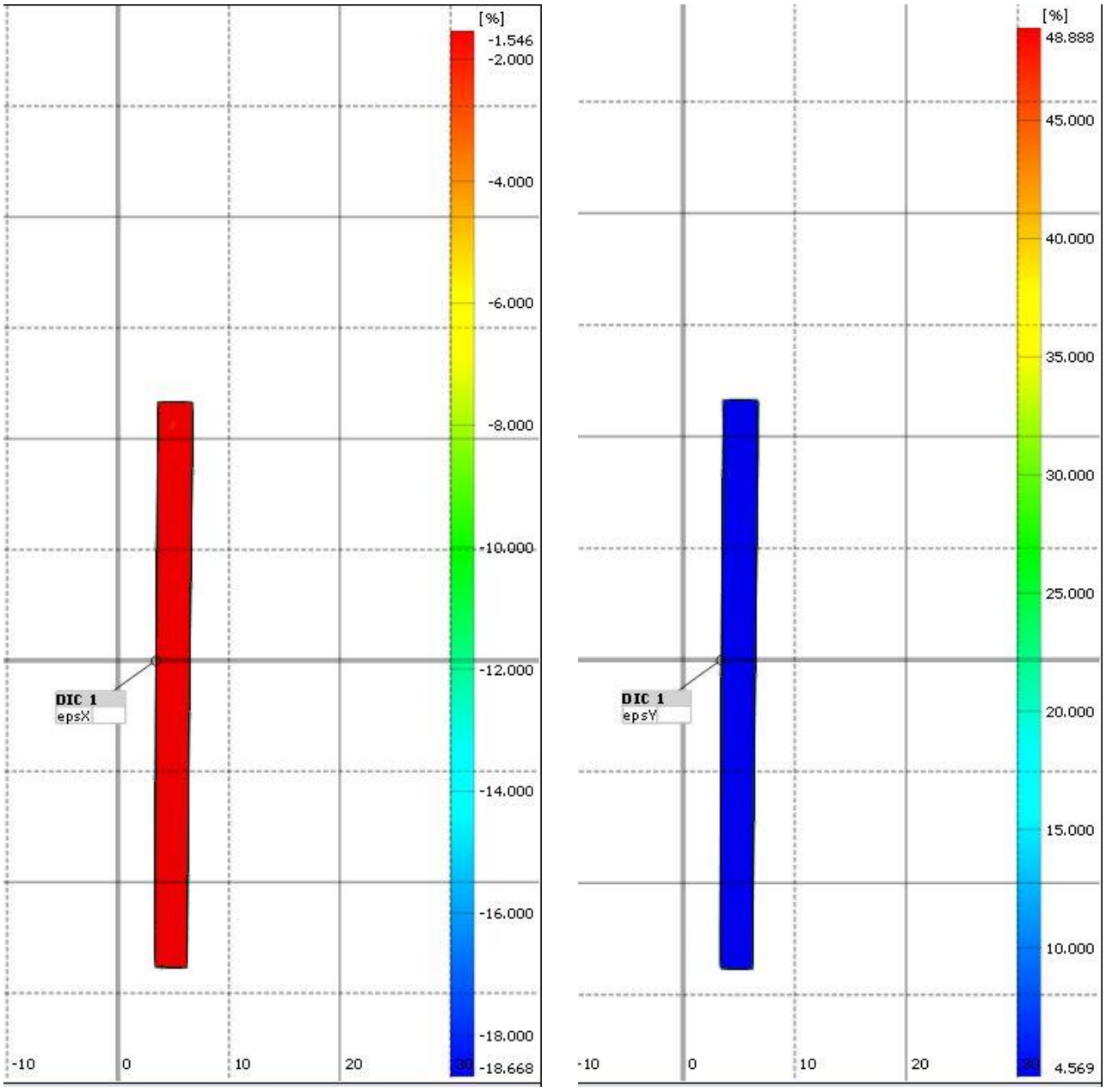

Figures 1-2: Strain components ε_{xx} and ε_{yy}, respectively, from the DIC analysis of 1018 Steel. Snapshots taken at frame 100, before yielding.

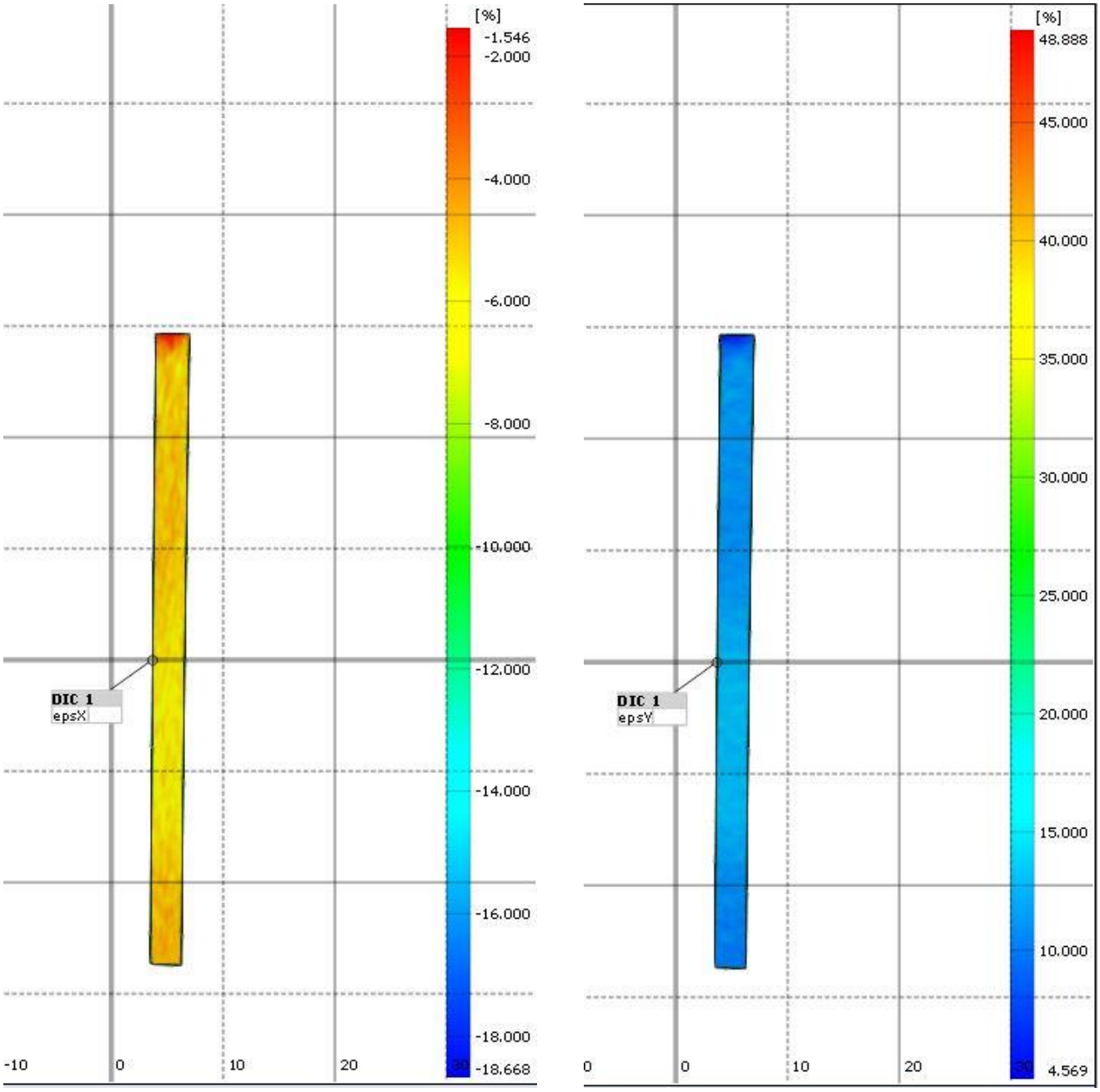

Figures 3-4: Strain components ε_{xx} and ε_{yy}, respectively, from the DIC analysis of 1018 Steel. Snapshots taken at frame 300, just after yielding.

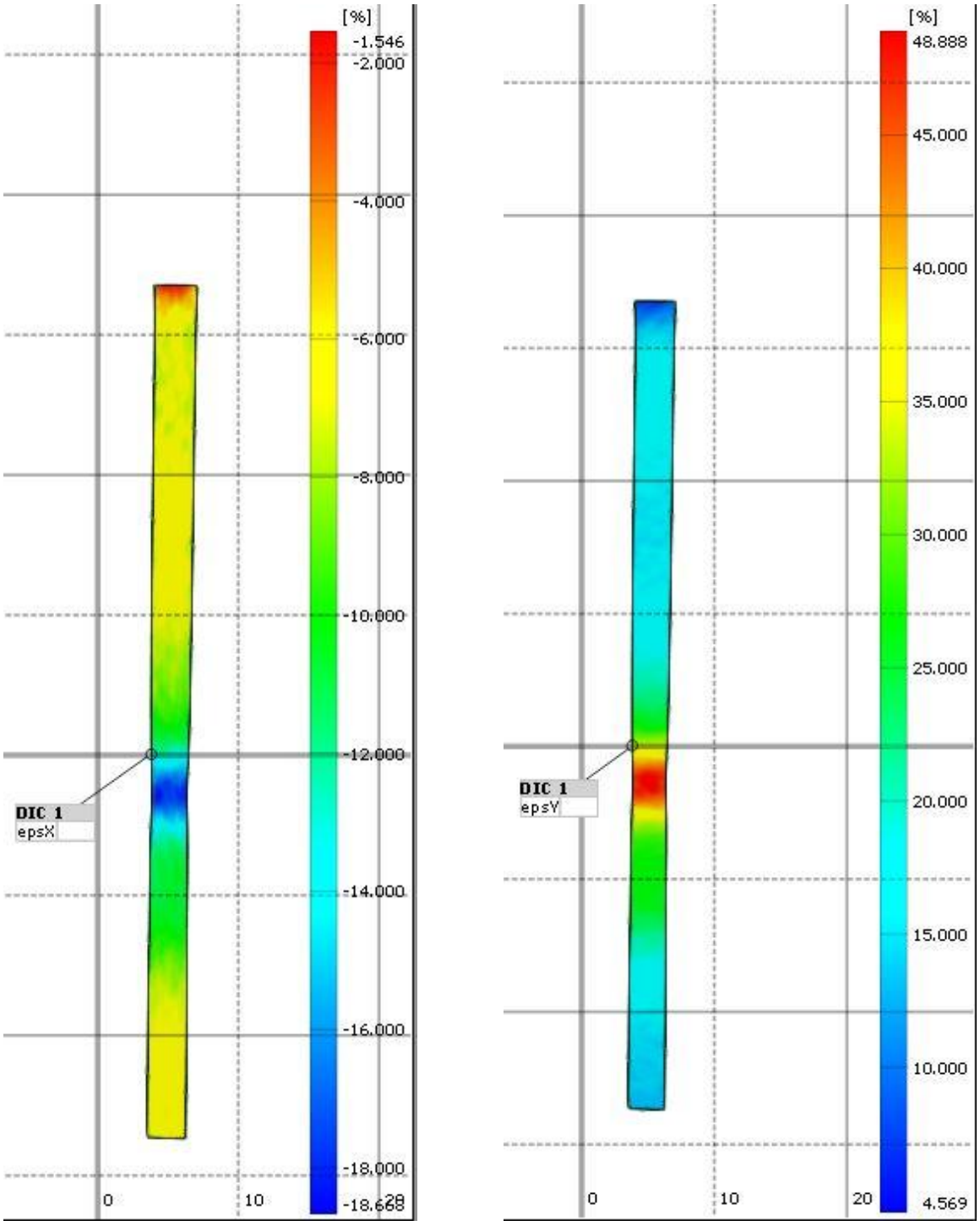

Figures 5-6: Strain components ε_{xx} and ε_{yy}, respectively, from the DIC analysis of 1018 Steel. Snapshots taken at frame 438, just before fracture.

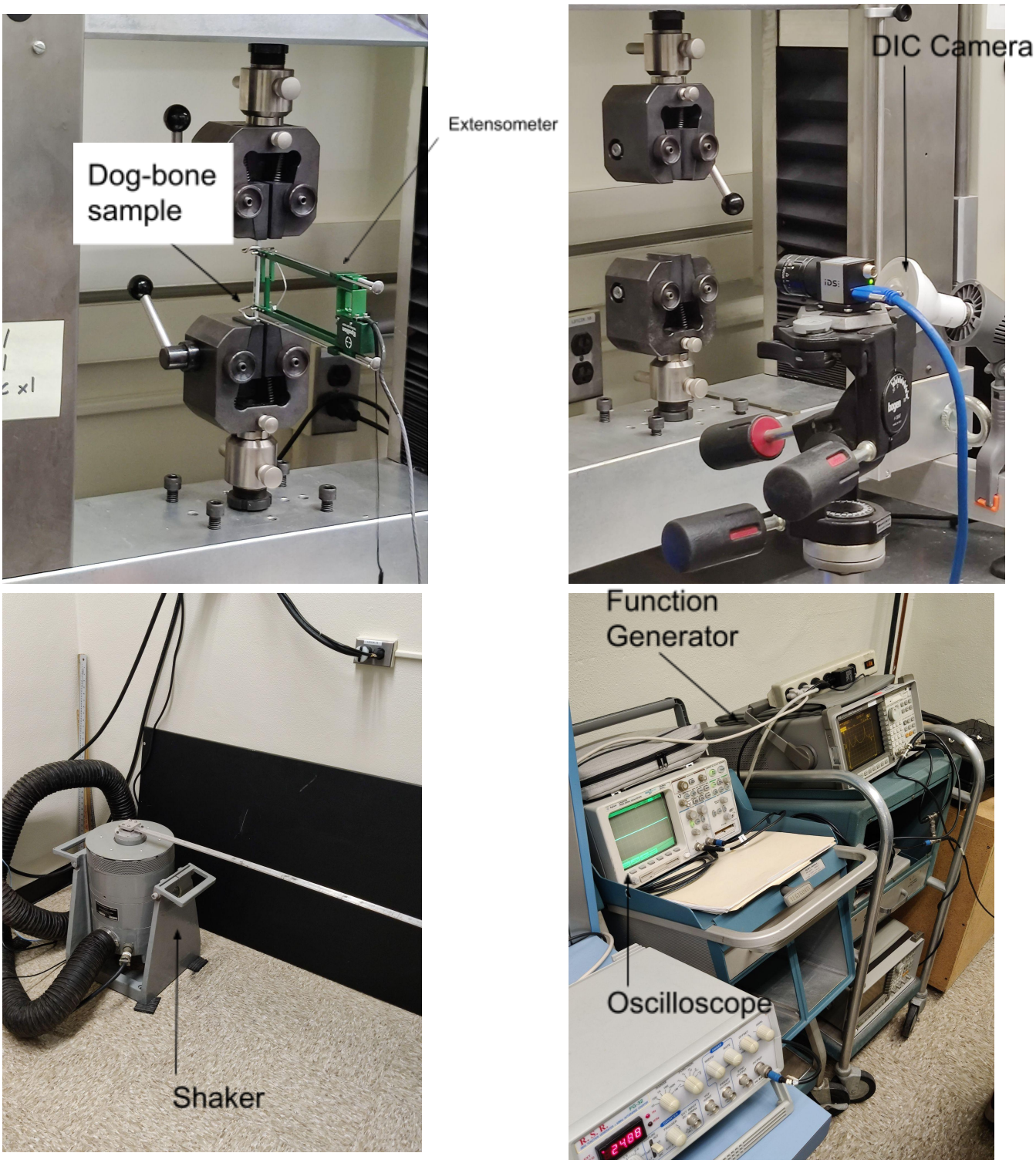

Figures 7-10: Images of the experiment area. Image credits: Trevor Burgoyne.